Eur. Phys. J. A **1**, 275–283 (1998)

THE EUROPEAN PHYSICAL JOURNAL A

β-decay half-lives of very neutron-rich isotopes of elements from Ti to Ni*

F. Ameil[1,2], M. Bernas[1], P. Armbruster[2], S. Czajkowski[3], Ph. Dessagne[4], H. Geissel[2], E. Hanelt[5], C. Kozhuharov[2], C. Miehe[4], C. Donzaud[1], A. Grewe[5], A. Heinz[5], Z. Janas[6], M. de Jong[5], W. Schwab[2], S. Steinhäuser[5]

[1] Institut de Physique Nucléaire d'Orsay, IN2P3-CNRS, F-91406 Orsay cedex, France
[2] Gesellschaft für Schwerionenforschung, Planckstraße 1 D-64220 Darmstadt, Germany
[3] Centre d'Etude Nucléaire de Bordeaux-Gradignan, IN2P3-CNRS, BP 120 F-33175 Gradignan Cedex, France
[4] Institut de Recherches Subatomiques, IN2P3-CNRS BP28 F-67037 Strasbourg cedex 2, France
[5] Institut für Kernphysik, Technische Hochschule Darmstadt, Schloßgartenstraße 9, D-64289 Darmstadt, Germany
[6] Instytut Fizyki Doświadczalnej, Uniwersytet Warszawski, Hoża 69 PL-00681 Warszawa, Poland

Received: 1 October 1997
Communicated by V. Metag

Abstract. The unknown β-decay half-lives of 22 isotopes far off stability ($5 < T_Z < 10$) in the region from Ti to Ni were measured at GSI, Darmstadt. The nuclei were produced in a fragmentation reaction of 500 A.MeV ^{86}Kr-projectile impinging on a thick Be target. The isotopes of interest were separated and identified with the fragment separator, FRS, by a combination of Bρ, Z, and ToF techniques. An additional range separation was performed by a selective implantation into granular detectors. The spatial and time correlations of the implant with the consecutively detected β-particles were used to determine the unknown half-lives. For nuclei far off stability, β-decay chains were measured and analyzed as well, leading to an even more reliable evaluation of the lifetimes. The large discrepancies found between the measured and the theoretical values emphasize that most recent theoretical work is not an improvement over calculations made almost a decade ago.

PACS. 23.40.-s β decay, double β decay, electron and muon capture – 27.30.+t $20 \leq A \leq 38$ – 27.50.+e $59 \leq A \leq 89$

1 Introduction

The extension of knowledge of half-lives to very neutron rich species provides a test of nuclear models far from stability. Although a global parameter, it is sensitive to low-lying β strength. For instance, new regions of deformation have been inferred from the evolution of measured β-decay properties as compared to experimental values in the region of n-rich Rb [1] or S [2]. For increasing Q_β values, significantly shorter half-lives and, conversely, the increase of neutron emission probabilities are expected. The parameters of the decay enter in the r-process calculations for the mass abundance of the nuclei beyond iron in the solar system. The occurrence of the r-peak at A = 80 demonstrates indeed the role of the neutron shell closure at N = 50 in the nucleosynthesis processes [3].

The identification of isotopes far from stability in projectile fragmentation requires the combination of a high luminosity spectrometer with a detection method optimized for the rejection of parasitic ions. Since the count rates become extremely low for isotopes at the limits of a possible identification, we chose to measure the β-decay half-lives $T_{1/2}$, the first and easiest nuclear quantity to measure in this context. Comparisons to values calculated with the QRPA approximation or with the Gross theory, recently revised, illustrate the limits of the models and the need for measurements.

Projectile fragmentation of high energy ^{86}Kr delivered by the heavy ion synchrotron SIS at GSI was investigated in a previous experiment [4]. The fragments were separated and analyzed using the fragment separator FRS [5]. In the Fe-region, the production yields and count rates were found to be large enough for measurements of β-decay half-lives.

In a pioneering experiment [6], we succeeded to separate and selectively implant ^{65}Fe-fragments in a thin layer of a granular Si-detector and to determine the unknown half-life of this isotope. We improved the method and extended it to twenty two neutron-rich isotopes with unknown half-lives in the vicinity of Fe. It should be noted that these elements are not efficiently extracted from the present day Isolde-type ion-sources and, hence, cannot be studied with on-line separation techniques.

* This work is part of the Ph. D. thesis of F. Ameil

2 Experimental set-up and fragments selection

2.1 Production

The ^{86}Kr-ions were delivered by the GSI heavy ion synchrotron, with an energy of 500 A.MeV. They came by spills of 80 ms width with a repetition rate of 0.3 per second. During the experiment the beam intensity was increased from $5 \cdot 10^7$ to 10^9 ions/spill, due to the dedicated efforts of the accelerator crew.

Be was chosen as target material, in order to optimize the number of reactions for a given momentum broadening of the merging fragments. The 2 g/cm^2 target thickness introduces a 2.4 to 3.4% momentum spread for Ni to V fragments respectively, slightly larger than the 2% momentum acceptance of the FRS.

2.2 Ionic separation and isotopic identification

The magnetic selection of the neutron-rich isotopes was performed with the fragment separator, FRS [5], see Fig. 1. At relativistic energies, the velocity of fragments is practically the same as the beam velocity ($\beta = 0.76$), and the atomic charge of the elements nearby Fe is q = Z. The two first dipoles, D1 and D2 (see Fig. 1), were tuned to a high magnetic rigidity to select large A/Z nuclei. The energy loss of the fragments in matter is a function of their nuclear charge Z and of their momentum. The separation in Z was achieved by slowing-down the transmitted fragments in an Al-degrader located in the intermediate dispersive focal plane, F2 and by tuning the second half of the FRS on a given ion. The thickness (roughly half of the range R of the ions of interest) and the angle of the wedge-degrader are adjustable [7]. For our measurements the mean degrader thickness was kept at 7 g/cm^2. Only the angle was adjusted for each isotope in order to maintain the isorange condition for the wanted isotope. This condition is fulfilled when the variation in thickness compensate the momentum dispersion of the ion of interest. The second half of the FRS (dipoles D3 and D4) was tuned on the rigidity of this isotope. At the exit of the FRS in F4, ions were focussed in velocity but distributed over 0.5 to 1 cm vertically and 15 cm horizontally. Around nine different nuclear species were simultaneously transmitted.

Those fragments were identified event-by-event along the second half of the FRS by the B$\rho \times \Delta$E $\times$ ToF (see Fig. 2a). The energy-losses ΔE were measured in a MUltiple-Step Ionization Chamber, MUSIC [8], at the exit of the last magnet. Since the velocities were equalized, the elements were directly Z-identified from the ΔE signals. The time of flight (ToF) was obtained from two plastic scintillator detectors located in the focal planes F2 and F4: the delayed STOP located in the intermediate dispersive focal plane F2, after the wedge degrader and the START, at the exit focus of the FRS, after the MUSIC chamber.

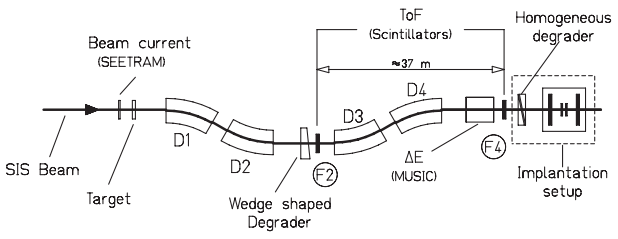

Fig. 1. FRS and detector setup for implantation and β-decay half-life measurements

2.3 Range selection

The 6 to 9 neighboring isotopes simultaneously transmitted have slightly different energies and ranges. Thus, the isotopic selection was completed by using this range difference. The thickness of a second homogeneous Al-degrader was chosen in such a way, that the fragments of interest, after passing through an active degrader (AD), would be selectively implanted in a thin PIN-diode. A 5 mm thick scintillator was chosen as an active degrader (AD). It was positioned in front of the PIN-diodes, in order to reduce the consequences of the angular straggling which blurred the vertical focusing in the previous experiment. As compared with Al, its material restrains the production of parasitic δ electrons. The ion-implantation and β detection were performed in each of the 20 Si chips of $10 \times 10 \times 0.500$ mm mounted in two rows of ten units. Behind the PIN-diodes, a scintillator similar to the AD was used as a veto detector for the fragments. The efficiency of the range-selection is illustrated on Fig. 2.

The granular detecting system reduces the β background, which comes mostly from the environment. The signals from the PIN-diodes were registered through a double amplification chain [6], β-signals being smaller than ions-signals by 4 orders of magnitude. Note that, for $T_{1/2} \sim 100$ ms the Q_β reaches ~ 10 MeV and only a very small fraction of the electron energy is deposited in the PIN-diodes.

However conversion electrons with energies up to ~ 500 keV can be fully stopped in the PIN diodes. The present device was also used to look for isomeric states which might decay via internal conversion (IC). As mentioned before, the isotopes are produced totally stripped. If isomeric states are populated, they cannot decay via IC, i.e. the isomeric life-time is prolonged due to the lack of bound electrons. Nuclei in these states would be implanted in the PIN-diodes, where the electronic shell vacancies are filled and, hence, the IC process becomes possible. Therefore, if such isomeric states were produced, a sharp peak in β energy spectra would be visible. At the present level of statistics no such peaks were observed.

2.4 Result of the ion-implantation

The identification of ^{66}Fe by range selection of fragments illustrates the method. Fig. 2a shows separated fragments detected together with ^{66}Fe in the F4 scintillator detector,

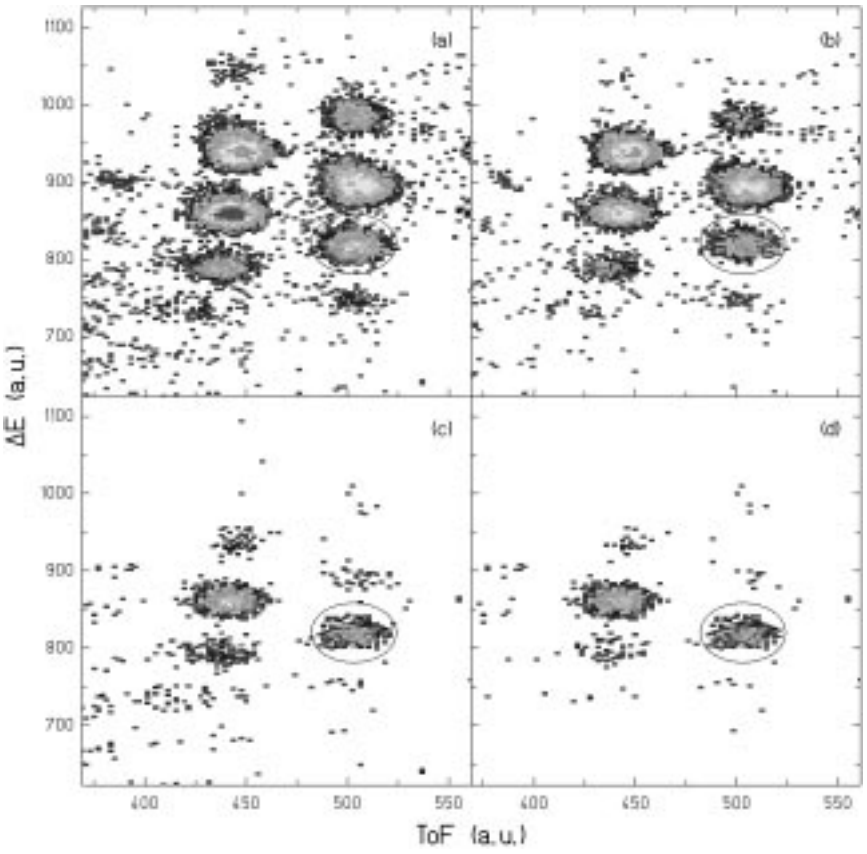

Fig. 2. Range selection in the case of the ^{66}Fe study: **a** ToF-ΔE Scatter-plot for all the ions transmitted at the final focal plane. **b** Ions stopped in the AD or in the frame of the PIN-diodes. **c** Ions hitting the PIN-diodes. **d** Ions implanted in the PIN-diodes

after the FRS. The rates provide an evaluation of yields, which compares well with the results of M. Weber et al. [4]. Additionally, the transmission of the FRS can also be checked [11]. In Fig. 2b the ΔE-ToF plot of fragments implanted in the AD or in the frame of the PIN diodes is shown. Fragments more ionizing than the investigated isotope are already stopped in the active degrader. Fig. 2c corresponds to particle-events hitting the PIN-diodes. Finally the veto rejects the more penetrating or secondary fragments produced in any of the degraders, and Fig. 2d shows the fragments implanted in the PIN-diodes. The two selected fragments which come out of the FRS with the same range are isotones. The investigated fragment, farther from the valley of stability, is the less intense of both, as confirmed by the simulation [10]. In many cases, the decay constant of the isotone was already known and related time correlations were used to determine the efficiency, ε, to detect the β-particle from the decay and the β-background rate, b, (see below). Since the accumulation rates of implants were often very low, less than one over ten spills and given the granularity of the detector, the contaminant β-activity did not interfere with the decay of interest.

Figure 3 shows the large neutron excess of the fragments under study. In case of ^{72}Co this excess reaches 13 units. In Table 1 are given the probability of neutron emission P_n as calculated by Möller [9] and the half-life of the daughter-decays T_f known from literature.

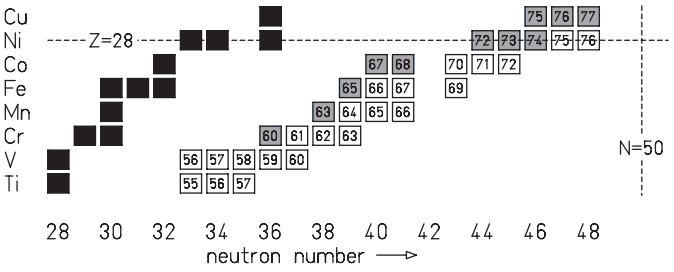

Fig. 3. Region of the chart of the nuclei where are shown (*white squares*) isotopes for which we measured half-lives. The isotopes for which we remeasured half-lives are indicated with *grey squares* and stable isotopes with *black squares*

3 Time correlation analysis

The decay constant, λ, of the implant is deduced from time-delayed correlations between the detection of the identified implant and the counting of the consecutive β-particles in the same PIN-diode. The distribution of time intervals is a function of λ, of the background b, of the β detection efficiency, ε and of the daughter decay half-life T_f. The last three parameters were determined with different methods so that the search could be concentrated on the only missing value of λ.

The background rate b/s/PIN-diode has to be determined as precisely as possible since b and λ are corre-

Table 1. Probability for β-delayed neutron emission P_n (from [9]) and daughter decay half-life T_f

	P_n %	T_f (s)		P_n %	T_f (s)		P_n %	T_f (s)		P_n %	T_f (s)
^{55}Ti	0	6.5	^{59}V	0	0.6	^{65}Mn	6.92	0.45	^{71}Co	2.61	1.86
^{56}Ti	0.06		^{60}V	0.03	0.57	^{66}Mn	10.88		^{72}Co	4.80	2.1
^{57}Ti	0.04		^{61}Cr	0.60	0.71	^{66}Fe	0	0.23	^{73}Ni	0.30	3.9
^{56}V	0	354	^{62}Cr	1.04	0.9	^{67}Fe	1.13	0.42	^{74}Ni	4.53	1.5
^{57}V	0	21	^{63}Cr	1.42	0.25	^{69}Fe	6.94	0.27	^{75}Ni	8.43	1.3
^{58}V	0	7	^{64}Mn	1.42	2	^{70}Co	2.51				

lated. It is evaluated by the random time distribution of a β signal with the next detected ion, i.e. reversing the time. This distribution was fitted to an exponential curve according to Poisson law, the slope of which gives b. An other method consists of building random-correlations between an implant in detector i and β's in detector $i+k$ for example.

However, for count rates larger than a few tenth of ions/pulse passing through the PIN-diodes, a beam pulsed background was measured coming from prompt δ electrons produced by the fast highly charged ions. Its contribution was suppressed by rejecting events from β spectrum with multiplicity larger than two. The mean value of b obtained as a result of the various methods is 0.1/s/detector. It is appropriate to look for half-lives of $T_{1/2} \lesssim 5$ s i.e. an apparent half-life of $\ln(2)/b$. Values related to each measurement are listed in Table 2.

Three methods were used to deduce the decay constant:

• The distribution of time intervals between the implant and the following detected β's in a time window $[0, T_c]$ was analyzed either with a χ^2 minimization or by the maximum likelihood calculation (MLH) using the probability density:

$$\rho(\lambda, \varepsilon, t) = b + \varepsilon\lambda \cdot e^{-\lambda t}$$

T_c being larger than $T_{1/2}$ by at least a factor 5.

• The distribution of time intervals between the implant and the first consecutive β detected was analyzed with the χ^2 minimization or MLH using the probability density:

$$\rho_1(\lambda, \varepsilon, t) = \varepsilon(\lambda + b) \cdot e^{-(\lambda+b)t} + (1-\varepsilon)b \cdot e^{-bt}$$

These expressions are completed by considering the daughter decay contribution [12], the half-lives of which are given in Table 1. Two examples of χ^2 minimizations are shown in Fig. 4. They illustrate the two methods of analyzing the same data set. In the first frame the first β after the implant is considered whereas in the second, all subsequent β's are involved.

• Very far from stability, Q_β values increase and half-lives decrease. Two or three β are emitted in cascade, and the chain occurs fast enough that short β time sequences can be identified, as long as the background rate remains low. For this purpose, we set a time window of approximately four times the expected half-life in order to select the time correlations related to these sequences. Their expected number is εN_F. We sorted out those for which a second β was detected in a short time interval: $\varepsilon^2 N_F$ sequences of two consecutive decays were then selected and so on. We evaluated the mean value of time intervals obtained at each step of the cascade. The mean time value was converted into $T_{1/2}$ including the correction due to the truncation by a time window [6]. In this way it was assumed that background events were rejected which is not 100% true; how reliable is this method was discussed and calculated in [11]. The higher level of confidence is found for the first decay in the cascade.

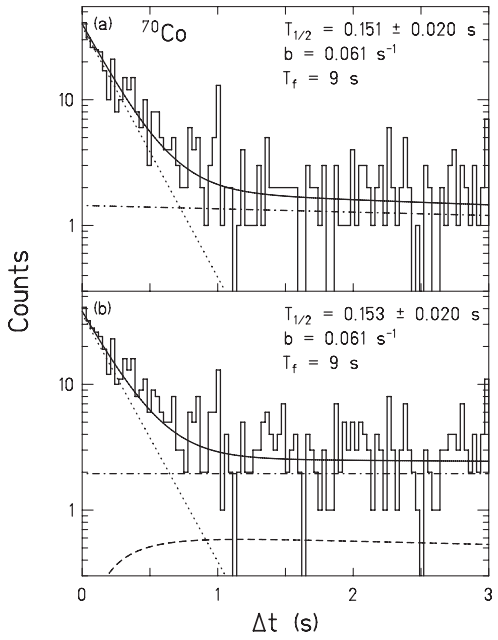

Fig. 4. Time difference spectra for ^{70}Co: **a** For the first β-particle detected after the implant and in the same PIN-diode. **b** For all β-particles detected after the implant and in the same PIN-diode. The *solid lines* represent the fitted curves, the *dotted lines* show the primary decay contributions, the *dashed-dotted lines*, the background contributions and the dashed line of Fig. b, the daughter-decay contribution (the unmeasured ^{70}Ni half-life, T_f, is taken as the mean value of several calculations)

After the last short decay, at the end of the sequence, the count-rate reflects the background and we checked that it was indeed compatible with the evaluations b previously mentionned. Two independent chains are reported in Fig. 5 to illustrate the results. The values of the daughter decay half-lives here obtained as well from mean time, provide a test of the method; for all decay chains they

Table 2. Parameters associated to each measurement; number of implants, background rate b, detection efficiency ε and results from the analysis of time correlations. For double measurements the sign † refers to the value obtained by analyzing the decay of the isotone of a more exotic nucleus and the sign ‡, the decay of the selected isotope

				χ^2 Analysis		MLH Calculation		Sequences	Results
	N_F	b (s^{-1})	ε	1^{st} β (s)	All β (s)	1^{st} β (s)	All β (s)	(s)	(s)
^{55}Ti	557	0.70 (2)	0.48 (6)	0.32 (6)					0.32 (6)
^{56}Ti	413	0.57 (1)	0.43 (5)	0.19 (4)					0.19 (4)
^{57}Ti	257	0.167 (5)	0.4 (1)			0.18 (3)	0.18 (4)	0.18 (2)	0.18 (3)
^{56}V	2196	0.70 (2)	0.5 (1)	0.24 (4)					0.24 (4)
^{57}V	2833	0.57 (1)	0.55 (10)	0.34 (8)					0.34 (8)
^{58}V	1586	0.167 (5)	0.32 (2)	0.20 (2)	0.21 (2)				0.20 (2)
^{59}V	607	0.111 (3)	0.30 (5)	0.12 (2)	0.15 (2)				0.13 (2)
^{60}V	289	0.103 (3)	0.45 (10)			0.18 (4)	0.22 (3)	0.21 (2)	0.20 (4)
^{61}Cr	1539	0.103 (3)	0.36 (3)	0.26 (2)	0.28 (2)				0.27 (2)
^{62}Cr	309	0.136 (3)	0.48 (10)	0.18 (2)	0.16 (2)	0,19 (2)	0,18 (2)	0,21 (2)	0.19 (3)
^{63}Cr	76	0.070 (3)	0.3					0.11 (7)	0.11 (7)
^{64}Mn†	918	0.070 (3)	0.32 (5)	0.12 (1)	0.17 (2)				0.13 (4)
^{64}Mn‡	667	0.095 (3)	0.35 (5)	0.14 (1)	0.20 (2)				0.16 (4)
^{64}Mn	*Final result obtained with two independant measurements*								0.14 (3)
^{65}Mn	276	0.045 (3)	0.45 (5)		0.10 (1)	0.12 (2)		0.12 (2)	0.11 (2)
^{66}Mn	146	0.047 (3)	0.45 (5)		0.09 (2)	0.09 (2)		0.07 (2)	0.09 (2)
^{66}Fe†	799	0.045 (3)	0.38 (4)	0.48 (3)	0.51 (4)				0.49 (4)
^{66}Fe‡	1099	0.128 (3)	0.23 (2)	0.39 (4)	0.38 (3)				0.38 (4)
^{66}Fe	*Final result obtained with two independant measurements*								0.44 (6)
^{67}Fe†	841	0.047 (3)	0.35 (10)	0.39 (5)	0.53 (6)				0.45 (8)
^{67}Fe‡	291	0.088 (3)	0.37 (10)			0.49 (7)	0.50 (7)	0.45 (6)	0.49 (7)
^{67}Fe	*Final result obtained with two independant measurements*								0.47 (5)
^{69}Fe	172	0.061 (3)	0.37 (3)			0.16 (3)	0.18 (3)	0.16 (3)	0.17 (3)
^{70}Co	1065	0.061 (3)	0.26 (3)	0.15 (2)	0.15 (2)				0.15 (2)
^{71}Co	282	0.067 (3)	0.45 (8)			0.22 (3)	0.21 (3)	0.23 (3)	0.21 (4)
^{72}Co	139	0.051 (4)	0.4 (1)			0.09 (2)	0.10 (2)	0.07 (2)	0.09 (2)
^{73}Ni	558	0.051 (4)	0.26 (4)	0.55 (8)	0.7 (1)				0.6 (1)
^{74}Ni	172	0.068 (4)	0.45 (9)			0.50 (9)	0.65 (16)	0.53 (7)	0.54 (16)
^{75}Ni	54	0.037 (4)	0.53					0.6 (2)	0.6(2)
^{76}Ni	3							$0.24^{+0.55}_{-0.19}$	$0.24^{+0.55}_{-0.19}$

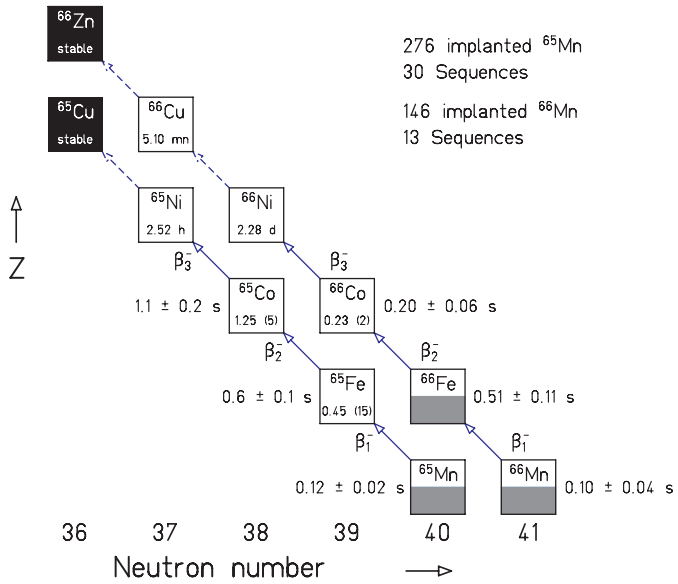

Fig. 5. Example of two β-decay chains with sequences of 3 fast β decays for the ^{65}Mn and ^{66}Mn

are indeed found to agree with values already published, which are indicated in the squares (see Fig. 5). Final error bars are due to the low statistics. Relevant sequences are selected at the price of a severe reduction of statistics. With this method, cascades of two or three decays were sorted out for the twelve most exotic isotopes listed in Table 2, except ^{76}Ni.

A bias may come from β-delayed neutron emission. A fraction of the decays from the isobaric line A would then move to line A−1. The β signal would be emitted by the (A−1 , Z+1) isotope (and so on) instead of (A , Z+1). However the probabilities of neutron emission remain small for the isotopes under investigation, as shown in Table 1 in which the calculated values of P_n are given [9]. They are smaller than a few % in most cases, small enough for our analysis to be valid.

4 Results of half-lives measurements

Half-lives obtained as a result of the different methods of analysis are given in Table 2. The error bars correspond

to statistical uncertainties and reflect the convergence of the few methods [11]. For low number of implanted fragments, statistical error dominates. However the selection of chains brought a nice confirmation of our statistical analysis. The extreme case of ^{76}Ni, observed for the first time and for which only three samples were implanted and one decay recorded leads to a value with a very large uncertainty. Uncertainty on the efficiency ε to detect the correlated β-particle also affects the $T_{1/2}$ accuracy. ε depends on the implantation depth −which was optimized in each setting− and on electronic thresholds for β-detection. It was not the same for all PIN's and indirect threshold effects on the triggers occurred. The pathological cases happened for isotopes the farthest from the ^{86}Kr projectiles and produced with the highest rates i.e. the closest from the stability valley. As seen in Table 2, the background there is large, associated with an apparent half-life of $\approx$ 1 s. For Ti and light V the uncertainty ranges between 20 to 30% since the pulsed background was a major problem.

The decay scheme is unknown for the considered isotopes. By assuming that the transition leads from g.s. to g.s., the decay constant can be noted as $\lambda \propto \langle i|M|f\rangle^2\, Q_\beta^5$. The first factor is the overlap of the initial and final nuclear states involved in the transition and the second is related with phase space. The $T_{1/2}$ values are plotted in Fig. 6 as function of Q_β (taken from [17]). Even with rather large error bars the results show a pronounced systematic behavior. The curve depicts half-lives versus Q_β, as a function $T_{1/2} = K{\cdot}Q_\beta^{-5}$, where K, the arbitrary normalization factor is different for each series of the same parity of the neutron number N.

The lines for N odd or even are found shifted with approximately the n-pairing energy i.e. 2.5 MeV. In the case of Ni for example, the odd N mother isotope is found with a similar half-life as the next even N nucleus but with a larger Q value since there is no neutron pair to break. Thus the Q_β values of odd N isotopes are systematically larger than for even N isotopes. The ^{68}Ni half-life does not fit so well but it is large and the delayed γ scheme is difficult to investigate [18]. For ^{70}Ni, both $T_{1/2}$ and Q_β were extrapolated from different calculations. The curve of even-N Ni isotopes provides the basis for extrapolating the ^{78}Ni half-life to a value of 100 ms. Even N Ni half-lives are well reproduced by recent microscopic calculations [16] as seen in Table 4.

The p-pairing energy appears also in this diagram when comparing the Q_β scales of odd and even Z elements. For the isotopes under scope which are in the same range of n-excess, the Q_β values are found larger for odd Z elements. The shift of 2 to 3 MeV towards larger Q_β for odd Z mother nuclei can be attributed to the gain in pairing energy for the last proton-pair in the final isotope.

The lack of variation of half-lives for odd N isotopes of very n-rich V does not follow the general trend. Q_β values, taken from [19], are slightly different from those of [17]. The discrepancy can be related with the 2 MeV difference in mass excess measured with TOFI [20] for ^{59}V and ^{60}V. However since the absolute Q_β values are large, mass excess uncertainties are not so critical.

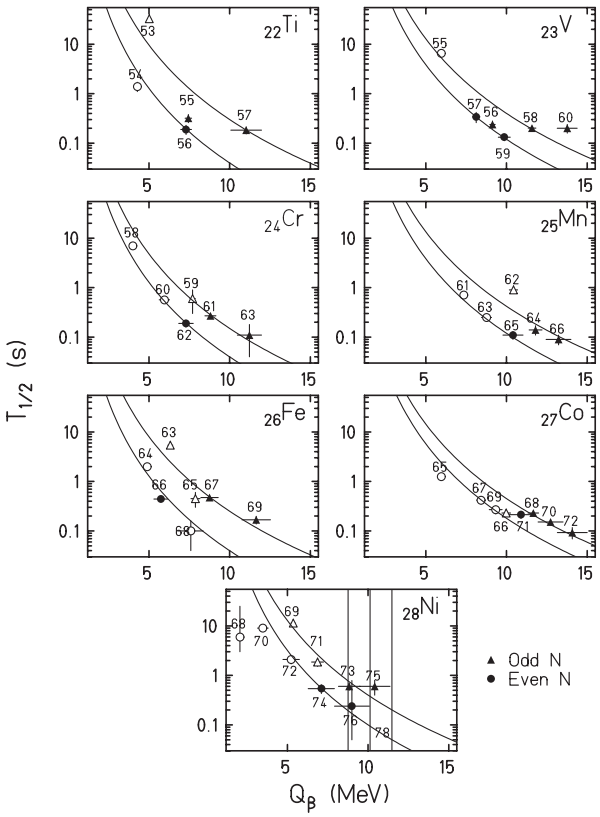

Fig. 6. Half-lives of n-rich isotopes as a function of Q_β taken from [17]. *Triangular* and *circular symbols* are assigned to odd and even neutron numbers respectively. Curves of $T_{1/2} \propto Q_\beta^{-5}$ are plotted with independent arbitrary normalizations. *Full symbols* are assigned to the half-lives measured in this work and *open symbols* to other measurements

5 Neutron-rich Ni nuclei

Whether double-shell closure effects survive very far off stability remains an open question. Recently the ^{28}O was demonstrated to be particle unbound [21] in spite of the double shell closure. The N=20 shell closure vanishes for a large excess of neutrons in the ^{32}Mg isotope [22] and the ground state was shown to be a deformed intruder state.

Today n-rich Ni isotopes become an accessible area to test nuclear models far off stability and ^{78}Ni offers an excellent case to try to answer the question. An experimental fact in favor of a strong N=50 shell closure effect in the region of interest is the observation of an r-process peak in the natural mass abundance distribution. The half-life of ^{78}Ni is extrapolated to 100 ms but it could be larger in the case of a strong shell closure effect as the Q_β would be reduced. Mass excesses, half lives, excited levels of heavier isotopes of Ni may already indicate the possible double shell closure.

Table 3. Measured half-lives of isotopes under study with values obtained from three different calculations

	$T_{1/2}^{exp.}$ (s)	$T_{1/2}^{th.}$ (s) Gr. Th. [13]	$T_{1/2}^{th.}$ (s) QRPA (Hilf) [14]	$T_{1/2}^{th.}$ (s) QRPA (FRDM) [15]
^{55}Ti	0.32 (6)	2.69	1.05	0.153
^{56}Ti	0.19 (4)	1.22	0.126	0.82
^{57}Ti	0.18 (3)	0.531	0.082	0.054
^{56}V	0.24 (4)	6.96	19.7	0.203
^{57}V	0.34 (8)	3.53	1.89	0.143
^{58}V	0.20 (2)	1.24	2.3	0.052
^{59}V	0.13 (2)	0.748	0.432	0.053
^{60}V	0.20 (4)	0.275	0.161	0.013
^{61}Cr	0.27 (2)	0.959	0.176	0.755
^{62}Cr	0.19 (3)	1.13	0.053	0.411
^{63}Cr	0.11 (7)	0.385	0.024	0.097
^{64}Mn	0.14 (3)	0.711	0.043	0.041
^{65}Mn	0.11 (2)	0.347	0.046	0.029
^{66}Mn	0.09 (2)	0.206	0.028	0.023
^{66}Fe	0.44 (6)	2.14	0.414	2.62
^{67}Fe	0.47 (5)	1.11	0.144	1.14
^{69}Fe	0.17 (3)	0.252	0.112	0.402
^{70}Co	0.15 (2)	0.268	0.103	0.047
^{71}Co	0.21 (4)	0.286	0.051	0.039
^{72}Co	0.09 (2)	0.113	0.054	0.032
^{73}Ni	0.6 (1)		0.806	2.90
^{74}Ni	0.54 (16)		0.462	1.99
^{75}Ni	0.6 (2)	0.432	0.242	1.04
^{76}Ni	$0.24^{+0.55}_{-0.19}$	0.311	0.141	0.956

6 Comparison of the deduced half-lives with calculated values

The values presently obtained are systematically compared with theoretical results in Table 3 and Fig. 7. The theoretical values are very scattered due to the increasing uncertainties on mass excess with the distance to the valley [23]. In case of V isotopes, the Q_β are not known for $A > 55$ [17] where the largest discrepancies are found.

The $T_{1/2}$ values calculated by T. Tachibana et al. [13] are usually too large except near the shell closure (e.g. Co and Ni) where the agreement is good, see Fig. 7a. However new calculations are in progress and improved values will be published soon. With the microscopic approach of A. Staudt et al. [14] values are under-estimated, see Fig. 7b, but mean value of half-lives agrees with our experimental results except for V.

The recent results predicted by P. Möller et al. [15], see Fig. 7c, do not converge either with experimental values. On the plot one can see an odd-even Z oscillation. Furthermore half-lives of even N isotopes are calculated too large. A detailed comparison indicates discrepancies as a function of neutron-pairing. The case of V isotopes shows within the three models a clear enhancement of the ratio with the mass number: it could point out the influence of deformed configurations.

Predicted half-lives decreasing too fast with n-excess indicate that the Q_β is increasingly overestimated see [25]. Even with most recent calculations of P. Möller and with the microscopic model of A. Staudt the predicted half-

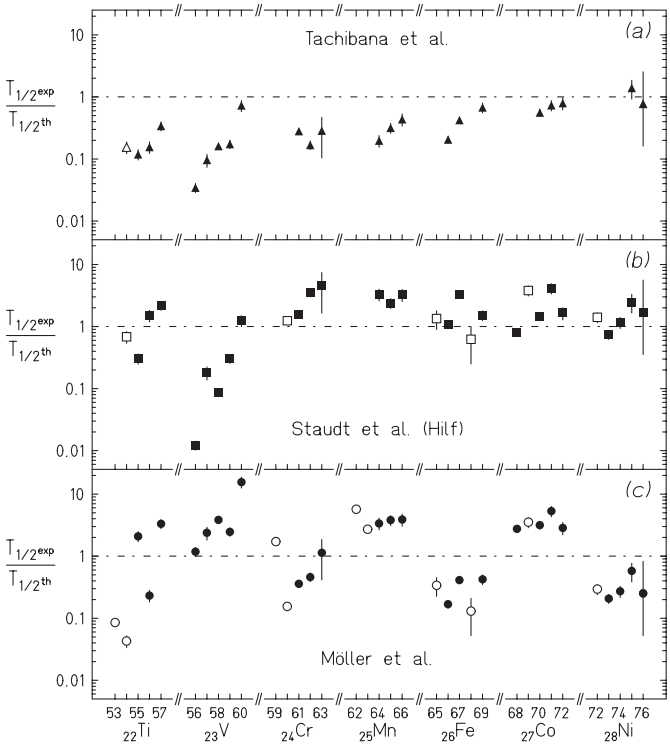

Fig. 7. Ratio of experimental half-lives over theoretical calculations. **a** For the revised Gross Theory calculations of Tachibana [13]. **b** For Staudt's microscopic calculations using QRPA [14] and the masses from Hilf [24]. **c** For the microscopic model of Möller using QRPA [15] and the FRDM [9] masses

Table 4. Comparison of measured half-lives for even Ni isotopes to recently calculated values [16]. For ^{78}Ni, not yet measured, the extrapolated half-life is indicated

	^{68}Ni	^{70}Ni	^{72}Ni	^{74}Ni	^{76}Ni	^{78}Ni
Measured $T_{1/2}$ (s)	18^{+6}_{-3}	–	2.1 ± 0.4	0.54 ± 0.16	$0.24^{+0.55}_{-0.19}$	(0.1)
Calculated $T_{1/2}$ (s) [16]	33	6.5	2.0	0.78	0.35	0.16

lives remain rather far from experimental values, this is why measurements are needed. Despite the difficulty of a comprehensive calculation of half-lives, in the specific case of even neutron-rich Ni isotopes, the values derived by J. Zylich [16] from Hartree-Fock calculations agree very well with the measured values (see Table 4).

7 Possible consequences for nucleosynthesis

The stellar nucleosynthesis of nuclei beyond Fe is usually attributed to the neutron capture process known as r and s-processes. Well defined peaks at A=80, 130 and 192 in the mass abundance distribution are finger prints of the r-process [3]. Sudden high flux of neutrons come with explosions of Super-Novae. The neutrons are captured by fusion residues, mostly ^{56,58}Fe nuclei. The temperature T is high and the r-process path corresponds to the fringe of isotopes for which the equilibrium of rates for (n,γ)$\leftrightarrow$(γ,n) takes place. The equilibrium is formulated in the nuclear Saha equation. When the r-process path follows increasing mass in a given element as for instance between ^{68}Ni and ^{78}Ni or between ^{60}Fe and ^{76}Fe, the abundances ratio of two adjacent isotopes depends exponentially on B_n/kT, B_n being the binding energy of the last neutron. Given odd-even differences in binding energies the equation leads to a temperature of 2.10^9 degrees, compatible with the accepted value. Then the r-process path follows the N=50 isotonic shell closure and the abundances ratio reflects the half-lives ratio as shown when delayed neutron emission probabilities remain negligible [26]. A more complete set of nuclear data, including the P_n and B_n for many more isotopes is required for reproducing solar mass-abundances distribution.

A few r-process sites with different neutron-densities and temperatures are needed to describe the global abundances curve. The synthesis of nuclei around the large peak of Fe may require other scenario like recently proposed with a neutrino wind [27], since very rare events may give sizable effects when involving the vast sidereal amount of Fe isotopes.

8 Conclusions and outlook

New β-decay half-lives of twenty-two very neutron-rich isotopes between Ti and Ni have been determined using time correlations between fragment and subsequent β-particles. Isotopes were produced by 500 A.MeV ^{86}Kr projectile fragmentation on a Be target at the SIS (GSI-Darmstadt) and separated with the FRS. The time correlations between the implantation of the fragment and the subsequent β-particles were analyzed to obtain the β-decay half-lives. The accuracy and quality of the result depend on the β detection efficiency ε and on the background b. The setup was designed to optimize the first parameter whereas the second was kept low enough so that half-lives smaller than 5 s could be measured.

However with $\varepsilon \sim 0.5$ and $b \sim 0.1$, the extraction of the half-life requires statistical analysis. For each measurement time spectra of the first β and of all β's emitted after the implant were analyzed by χ^2 minimization and MLH methods according to the number of ions.

Since isotopes investigated far-off stability have Q_β values up to 10 MeV, cascades of 2 to 3 β-decays occur in a time shorter than 5 s. Therefore decay-chains can be identified. This method, used for the first time in the frame of β-decays, reduces the number of significant sequences but provides an almost complete suppression of the background, mostly for the first decay. The requirement of a convergence on b, ε and $T_{1/2}$ from the different methods improves the confidence in the final values. Comparison with theoretical values shows discrepancies up to two orders of magnitude. The nuclear models to obtain Q_β and the β-decay calculations need further improvements to reproduce the data and to allow extrapolations. The half-lives depend mostly on the energy phase space i.e. Q^5 and the nuclear contributions have still to be investigated. Three ions of ^{76}Ni isotope were identified for the first time and a first decay was measured.

Half-lives and Q_β enter as ingredients in stellar nucleosynthesis calculations. Given the differences between calculated and measured values, improved calculations are needed to reproduce the sidereal mass abundances. Future investigations with respect to n-rich Ni may proceed by populating the isomeric states expected in n-rich Ni isotopes [28]. Already discovered in ^{68}Ni and ^{70}Ni their decay γ-spectra give access to low seniority states. It may offer the experimental access to the double shell closure effect in Ni^{78}.

In recent experiments on ^{238}U projectile-fission many very neutron rich fragments were separated for the first time [29] down to Ca and their production yields were measured. The present method well suited to low counting rates can be extended to these fragments. Mass excess will be measured in the storage ring for isotopes produced with the largest yields.

We wish to thank Professor G. Münzenberg for his friendly support to our project, K.-H. Behr, A. Brühnle, L. Petizon and G. Voltonini for their technical assistance and one of us (F.A.) the IN2P3/GSI for the fellowship allocated to this work.

References

1. J. Äystö, A. Astier, T. Enqvist, K. Eskola, Z. Janas, A. Jokinen, K.-L. Kratz, M. Leino, M. Penttilä, B. Pfeiffer and J. Zylicz: Phys. rev. Lett. **69** (1992) 1167
2. O. Sorlin, D. Guillemaud-Mueller, A. C. Mueller, V. Borrel, S. Dogny, F. Pougheon, K.-L. Kratz, H. Gabelmann, B. Pfeiffer, A. Wöhr, W. Ziegert, Y. E. Penionzhkevich, S. M. Lukyanov, V. S. Salamantin, R. Anne, C. Borcea, L. K. Fifield, M. Lewitowicz, M.-G. Saint-Laurent, D. Bazin, C. Détraz, F. K. Thielemann and W. Hillebrandt: Phys. Rev. **C47** (1993) 2941
3. E. M. Burbidge, G. R. Burbidge, W. A. Fowler and F. Hoyle: Rev. Mod. Phys. **29** (1957) 547
4. M. Weber, C. Donzaud, J.-P. Dufour, H. Geissel, A. Grewe, D. Guillemaud-Mueller, H. Keller, M. Lewitowicz, A. Magel, A. C. Mueller, G. Münzenberg, F. Nickel, M. Pfützner, A. Piechaczek, M. Pravikoff, E. Roeckl, K. Rykaczewski, M.-G. Saint-Laurent, I. Schall, C. Stephan, K. Sümmerer, L. Tassan-Got, D. J. Vieira and B. Voss: Zeit. für Phys. **A343** (1992) 67
5. H. Geissel, P. Armbruster, K.-H. Behr, A. Brünle, K. Burkard, M. Chen, H. Folger, B. Franczak, H. Keller, O. Klepper, B. Langenbeck, F. Nickel, E. Pfeng, M. Pfützner, E. Roeckl, K. Rykaczewski, I. Schall, D. Schardt, C. Scheidenberger, K.-H. Schmidt, A. Schröter, T. Schwab, K. Sümmerer, M .Weber, G. Münzenberg, T. Brohm, H.-G. Clerc, M. Fauerbach, J.-J. Gaimard, A. Grewe, E. Hanelt, B. Knödler, M. Steiner, B. Voss, J. Weckenmann, C. Ziegler, A. Magel, H. Wollnik, J.-P. Dufour, Y. Fujita, D. J. Vieira and B. Sherrill: Nucl. Instr. and Meth. **B70** (1992) 286
6. S. Czajkowski, M. Bernas, P. Armbruster, H. Geissel, Ch. Kozhuharov, G. Münzenberg, D. J. Vieira, Ph Dessagne, Ch Miehe, E. Hanelt, G. Audi and J. P. K. Lee: Zeit. für Phys. **A348** (1994) 267 and S. Czajkowski, Thèse Université Paris VII (1992): rapport IPNO-T-92-02 Orsay
7. K.-H. Schmidt, E. Hanelt, H. Geissel, G. Münzenberg and J.-P. Dufour: Nucl. Instr. and Meth. **A260** (1987) 287
8. M. Pfützner, H. Geissel, G. Münzenberg, F. Nickel, C. Scheidenberger, K.-H. Schmidt, K. Sümmerer, T. Brohm, B. Voss and H. Bichsel: Nucl. Instr. and Meth. **B86** (1994) 213
9. P. Moeller, J. R. Nix, W. D. Myers and W. J. Swiatecki: Atomic Data and Nuclear Data Tables **59** (1995) 185
10. Th. Schwab: Dissertation, GSI Report **91-10** (1991)
11. F. Ameil, Thèse Université Clermont-Ferrand II (1997): rapport IPNO-T-97-02 Orsay
12. M. Bernas, P. Armbruster, J.-P. Bocquet, R. Brissot, H. Faust, Ch. Kozhuharov and J.-L. Sida: Zeit. für Phys. **A336** (1990) 41
13. T. Tachibana, M. Yamada and K. Nakata: Report of Sciences and Engineering Research Laboratory **88-4** Waseda University (1988)
14. A. Staudt, E. Bender, K. Muto and H. V. Klapdor: Atomic Data Nuclear Data Tables **44**, (1990) 79
15. P. Möller, J. R. Nix and K.-L. Kratz: to be published in Atomic Data Nuclear Data Tables
16. J. Dobaczewski, Z. Szymanski and J. L. Zylicz: Workshop on nuclear fission and fission products spectroscopy, Seyssins (1994), edt by H. Faust and G. Fioni, ILL-Grenoble.
17. G. Audi and A. H. Wapstra: Nucl. Phys. **A565** (1993)
18. E. Runte, K.-L. Gippert, W.-D. Schmidt-Ott, P. Tidemand-Petersson, L. Ziegeler, R. Kirchner, O. Klepper, P.O. Larsson, E. Roeckl, D. Schardt, N. Kafrell P. Peuser, M. Bernas, P. Dessagne, M. Langevin and K. Rykaczewski: Nucl. Phys. **A441** (1985) 237
19. W. D. Myers and W. J. Swiatecki: Nucl. Phys. **A601** (1996) 141
20. D. J. Vieira, H. L. Seifert, J. M. Wouters, H. Wollnik, X. G. Zhou, Z. L. Tu, Z. Y. Zhou and G. W. Butler: ENAM 95, Edt frontieres, M. de Saint Simon and O. Sorlin, (1995) 103
21. O. Tarasov, R. Allatt, J. C. Angélique, R. Anne, C. Borcea, Z. Dlouhy, C. Donzaud, S. Grévy, D. Guillemaud-Mueller, M. Lewitowicz, S. Lukyanov, A. C. Mueller, Yu. Oganessian, N. A. Orr, A. N. Ostrowski, R. D. Page, Yu. Penionzhkevich, F. Pougheon, A. Reed, M. G. Saint-Laurent, W. Schwab, E. Sokol, O. Sorlin, W. Trinder and J. S. Winfield: Nuclear Physics at GANIL 1994-1995 (1995) 50
22. D. Guillemaud-Mueller, C. Détraz, M. Langevin, F. Naulin, M. de Saint-Simon, C. Thibault, F. Touchard, and M. Epherre: Nucl. Phys. **A426** (1984) 37
23. P. Haustein: AMCO-VII Conference (1984) 413, edt by O. Klepper, GSI Darmstadt, Germany
24. E. R. Hilf, H. von Groote and K. Takahashi: CERN Report **76-13** (1976) 142
25. S. Goriely and M. Arnoult: Astron. Astrophys. **262** (1992) 73
26. K.-L. Kratz, V. Harms, W. Hillebrandt, B. Pfeiffer, F. K. Thielemann and A. Wöhr: Zeit. für Phys. **A336** (1990) 357
27. S. E. Woosley, J. R. Wilson, G. J. Mathews, R. D. Hoffman, and B. S. Meyer: Astrophysical Journal **433** (1994) 229
28. M. Pfützner, R. Grzywacz, M. Lewitowicz and K. Rykaczewski: Proceedings of the 3rd International Conference on nuclear Physics at Storage Rings (STORI 96) (1996) to be published in Nucl. Phys. A
29. M. Bernas, P. Armbruster, S. Czajkowski, F. Ameil, P. Dessagne, C. Donzaud, C. Engelmann, H. Geissel, A. Heinz, C. Kozhuharov, C. Miehe, G. Münzenberg, M. Pfützner, C. Röhl, W. Schwab, C. Stéphan, K. Sümmerer, L. Tassan-Got and B. Voss: Nucl. Phys. **A616** (1997) 352c